Electronic Supplementary Material (ESI) for Chemical Communications.

Supporting Information

A C_{60}-aryne building block: Synthesis of a hybrid all-carbon nanostructure

D. García,[a] L. Rodríguez-Pérez,[b] M. A. Herranz,[b] D. Peña,[a] E. Guitián,[a] S. Bailey,[c] Q. Al-Galiby,[c,d] M. Noori,[c] C. J. Lambert,[c] D. Pérez*[a] and N. Martín*[b,e]

[a] *Centro de Investigación en Química Biolóxica e Materiais Moleculares (CIQUS) and Departamento de Química Orgánica, Universidade de Santiago de Compostela, Santiago de Compostela 15782 Spain. E-mail: dolores.perez@usc.es*

[b] *Departamento de Química Orgánica I, Facultad de Química, Universidad Complutense de Madrid, Avda. Complutense s/n, 28040 Madrid, Spain. E-mail: nazmar@ucm.es*

[c] *Physics Department, Lancaster University, LA1 4YB Lancaster, United Kingdom*

[d] *Physics Department, College of Education, Al-Qadisiyah University, IRAQ*

[e] *IMDEA-Nanociencia, c/Faraday 9, Campus Cantoblanco, 28049 Madrid, Spain*

Experimental Section

Materials and Methods. All reactions were carried out under argon using oven-dried glassware. PhCl and TMSCl were dried by distillation from CaH_2, Tf_2O was distilled and stored under argon and CH_3CN was purified by an MBraun SPS-800 Solvent Purificarion System. Other solvents and reagents used in this work were purchased from commercial suppliers and used as received. Bistriflate **1** was prepared following a modification of a previously published procedure.[1] An anhydrous stock solution of TBAF (1M in CH_3CN) was prepared as described in the literature.[2] TLC chromatography was performed on Merck silica gel 60 F254 plates; chromatograms were visualized with UV light (254 and 360 nm). Flash column chromatography was performed on Merck silica gel 60 (ASTM 230-400 mesh).

Graphite from TIMCAL (TIMREX SFG15, ρ = 2.26 g/cc, particle size = 8.80 µm, specific surface = 9.50 m^2/g, ashes ≤ 0.100%, interlamellar distance = 3.354-3.358 Å) was used for the synthesis of few layer graphene (FLG). For the exfoliation of **graphene**, graphite flakes (200 mg) were dispersed in anhydrous *o*-DCB (200 mL) and sonicated at a low-power sonication bath for 150 minutes under inert atmosphere. The dispersion was centrifuged at 500 rpm for 45 minutes, the supernatant was decanted and stored in solution.[3] TEM images showed FLG nanosheets of less than 5 layers staked with smaller flakes on their surface (Fig. S1). Lateral dimensions of the nanosheets range from 100 to 500 nm. Raman spectroscopy (532 nm laser excitation wavelength) confirms the pristine graphitic structure of graphene produced from *o*-DCB and the presence of less than 5 layers (deconvolution of the 2D band in 6 Lorentzianes with FWHM = 24 cm^{-1}). The relatively low D-band intensities provide evidence of few defects on the FLG surface (Fig. S8).

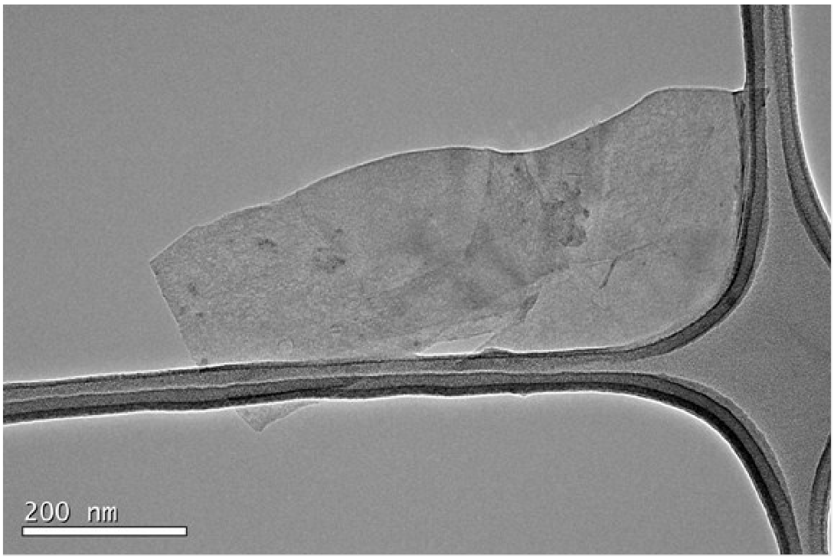

Fig. S1 TEM image of the FLG obtained from the exfoliation of graphite flakes in *o*-DCB.

Instruments. ^1H NMR and ^{13}C NMR spectra were recorded at 300 and 75 MHz (Varian Mercury-300 instrument), 500 and 125 MHz (Varian Inova 500) or 700 and 175 MHz (Bruker AVIII 700 MHz), respectively. MALDI-TOF spectra were determined on a Bruker Autoflex instrument. TGA analyses were carried out under nitrogen in a TA-TGA-Q500 apparatus. The sample (~ 0.5 mg) was introduced inside a platinum crucible and equilibrated at 100 ºC followed by a 10 °C min^{-1} ramp between 100 and 1000 °C followed by an isotherm of 30 minutes. FTIR spectra were carried out in a Bruker

TENSOR 27 using a spectral range was 4000-400 cm^{-1}, with a resolution of 1 cm^{-1}, and in pellets of dispersed samples of the corresponding materials in dried KBr. Raman spectra were recorded on a NT-MDT-in Via Microscope at room temperature using an exciting laser source of 532 nm. XPS analyses were carried out using a SPECS GmbH (PHOIBOS 150 9MCD) spectrometer operating in the constant analyzer energy mode. A non monochromatic aluminium X-ray source (1486.61 eV) was used with a power of 200 W and voltage of 12 kV. Pass energies of 75 and 25 eV were used for acquiring both survey and high resolution spectra, respectively. Survey data were acquired from kinetic energies of 1487 - 400 eV with an energy step of 1 eV and 100 ms dwell time per point. The high resolution scans were taken around the emission lines of interest with 0.1 eV steps and 100 ms dwell time per point. SpecsLab Version 2.48 software was used for spectrometer control and data handling. The semi-quantitative analysis were performed from the C 1s (284.3 eV) signal. The samples were introduced as pellets of 8 mm diameter. TEM micrographs were obtained using a JEOL 2100 microscope operating at 200 kV. The samples were dispersed in *o*-DCB and dropped onto a holey carbon copper grid (200 mesh), the solvent was removed in a vacuum oven during 48 h. AFM images were obtained by a Park Systems NX-10 microscope operating in True Non-Contact^{TM} mode, with independent XY scanner (10 µm x 10µm, resolution 0.05 nm) and Z scanner (resolution 0.015 nm, position detector noise 0.03 nm), using high resolution SSS-NCHR tips, with nominal radius of curvature of 2.5 nm (maximum < 5 nm). The samples were dispersed in *o*-DCB, sonicated for 150 min, centrifuged at 5000 rpm for 15 min, and the supernatant was deposited on freshly cleaved mica substrate by spin-coating; the solvent being removed by heating at 60 ºC under vacuum for 48 h.

Synthesis of *o*-(trimethylsilyl)aryl triflate 2

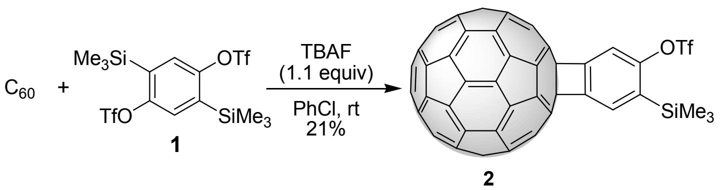

To a solution of 2,5-bis-(trimehylsilyl)-1,4-phenylene bis(trifluoromethanesulfonate) (**1**) (173 mg, 0.33 mmol) and C_{60} (120 mg, 0.17 mmol) in PhCl (17 mL), anhydrous TBAF (1M solution in CH_3CN, 330 µL, 0.33 mmol) was dropwise added over a period of 2 h (syringe pump). The mixture was stirred at rt for 2 h. The solvent was evaporated under reduced pressure and the resulting mixture was purified by column chromatography (SiO_2, CS_2) to afford *o-(*trimethylsilyl)aryl triflate **2** (35 mg, 21%) as a dark solid.

^{1}H NMR (500 MHz, $CDCl_3$), δ: 8.15 (s, 1H), 7.99 (s, 1H), 0.59 (s, 9H); ^{13}C NMR (125MHz, $CDCl_3$), δ: 155.9, 153.9, 153.7, 151.3, 148.4, 146.9, 146.2, 146.2, 145.6, 145.5, 145.5, 145.5, 145.3, 144.6, 143.1, 143.0, 142.9, 142.9, 142.4, 142.4, 142.0, 141.9, 140.6, 139.2, 139.0, 135.7, 131.4, 118.8 (q, *J* = 325 Hz, CF_3), 115.3, -0.41; EM (MALDI-TOF), *m/z* (%): 1016.015 (M^+, 37), 1017.016 (M^++1, 45), 1018.015 (M^++2, 45), 720 (100); FTIR (KBr): ν = 2957, 2924, 2854, 1424, 1215, 1140, 997, 941, 890, 862, 843, 526 cm^{-1}.

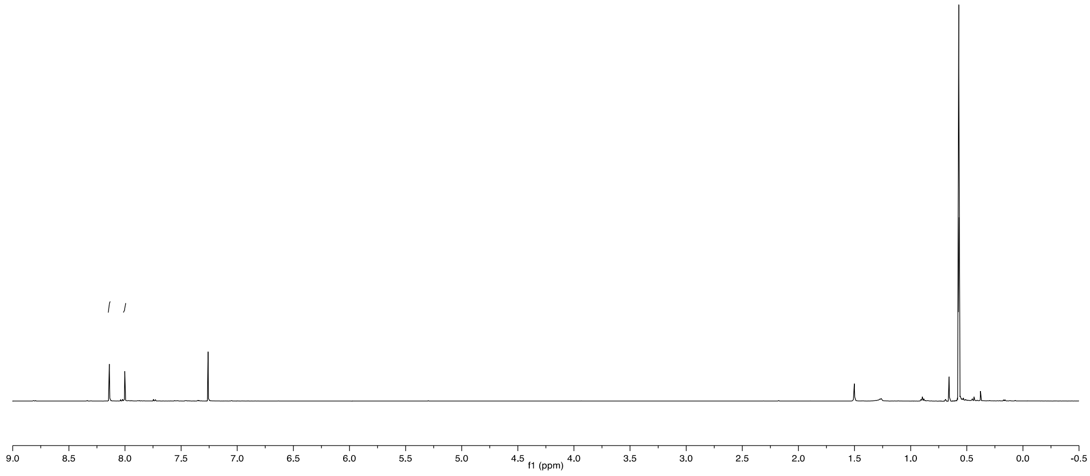

Fig. S2 ^{1}H NMR spectrum (500 MHz, $CDCl_3$) of **2**.

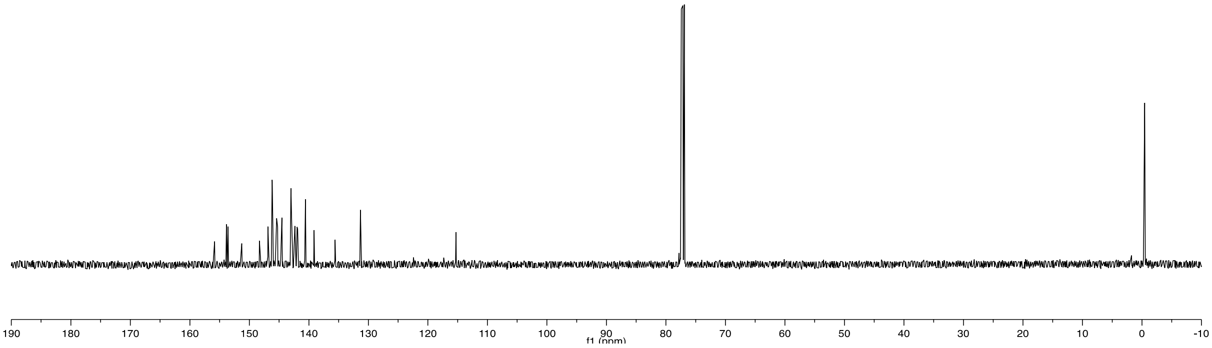

Fig. S3 ^{13}C NMR spectrum (125MHz, $CDCl_3$) of **2**.

Generation of *fullerobenzyne* 3

To a solution of the *o*-(trimethylsilyl)aryl triflate **2** (30 mg, 0.03 mmol) in dry *o*-DCB (20 mL), anhydrous TBAF (1M solution in CH_3CN, 85 μL, 0.6 mmol) was dropwise added over a period of 2 h. The solution was stirred vigorously at rt for 2 h. After this period of time, a brown solid was obtained by filtration over a PTFE membrane (0.1

µm). The solid was washed in the membrane with *o*-DCB, toluene, CH_2Cl_2, MeOH and H_2O to remove the excess of TBAF, since all the *o*-(trimethylsilyl)aryl triflate **2** was consumed as confirmed by TLC analysis. The obtained solid was suspended in CS_2 and analyzed by MALDI-TOF mass spectrometry. A complex mixture (multiadducts and small oligomers that also contain fluorine) with molecular weights up to 3400 u was observed (Fig. S4).

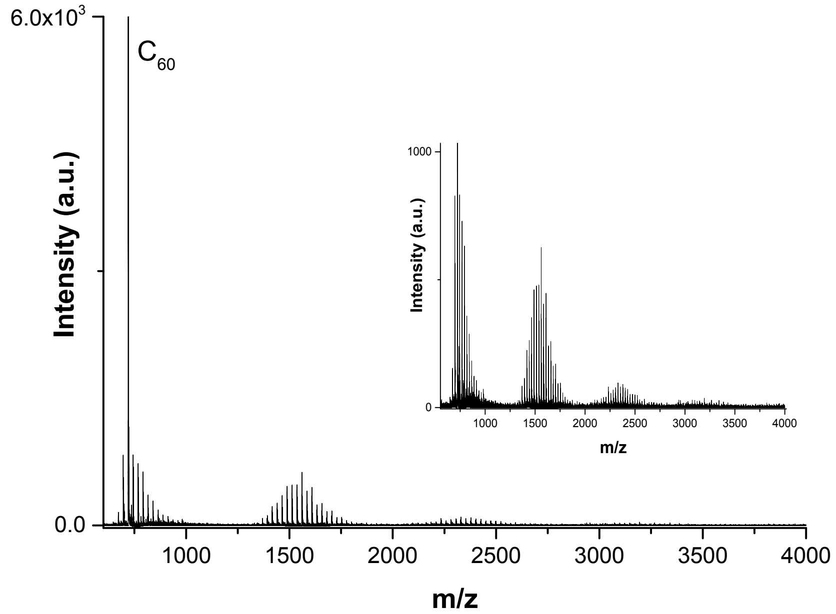

Fig. S4 EM (MALDI-TOF) of the solid obtained by reaction of *o*-(trimethylsilyl)aryl triflate **2** with TBAF in *o*-DCB.

Generation of *fullerobenzyne* 3 and trapping with C_{60}

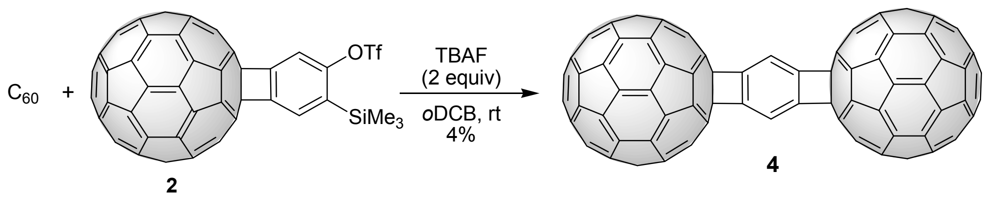

2

4

To a solution of the *o*-(trimethylsilyl)aryl triflate **2** (30 mg, 0.03 mmol) and C_{60} (84 mg, 0.46 mmol) in dry *o*-DCB (20 mL), anhydrous TBAF (1M solution in CH_3CN, 85 µL, 0.6 mmol) was dropwise added over a period of 2 h. The solution was stirred vigorously at rt for 2 h. After this period of time, a brown solid was separated from the reaction mixture by filtration over a PTFE membrane (0.1 µm). The solid was washed in the membrane with *o*-DCB, toluene, CH_2Cl_2, MeOH and H_2O to remove the excess of reactants. The final solid was suspended in CS_2, sonicated and centrifuged. A mixture of multiadducts was identified in the precipitated at the centrifuge tube by mass spectrometry. Product **4** remained in solution and was isolated after solvent evaporation (2 mg, 4%). Due to the extreme insolubility of dumbbell **4**, the spectroscopic characterization was achieved only with partial resolution (^{13}C NMR).

^{1}H NMR (700 MHz, $CDCl_3$), δ: 8.90 (s, 2H); ^{13}C NMR (175MHz, $CDCl_3$), δ: 154.5, 147.1, 146.5, 146.4, 146.0, 145.9, 145.8, 145.7, 144.9, 144.8, 143.5, 143.4, 143.3, 142.7, 142.5, 141.0, 140.8, 139.4, 120.0; EM (MALDI-TOF), *m/z* (%): 1514.004 (M^+, 15); 1515.016 (M^++1, 30); 1516. 020 (M^++2, 28); FTIR (KBr): ν = 2956, 2922, 2851, 1626, 1461, 1461, 1123, 1068, 1033, 874, 722, 526 cm^{-1}.

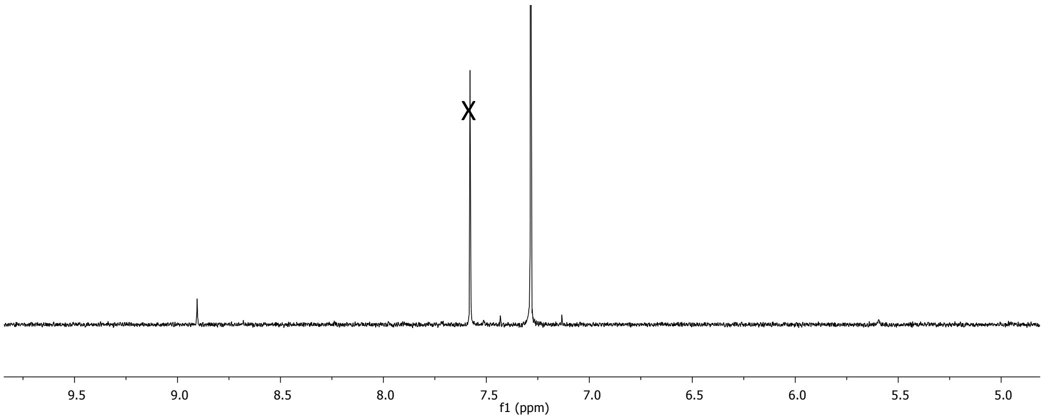

Fig. S5 ^{1}H NMR spectrum (700 MHz, CS_2 with $CDCl_3$ as internal reference) of **4**. Traces of benzene contained in the CS_2 were detected.

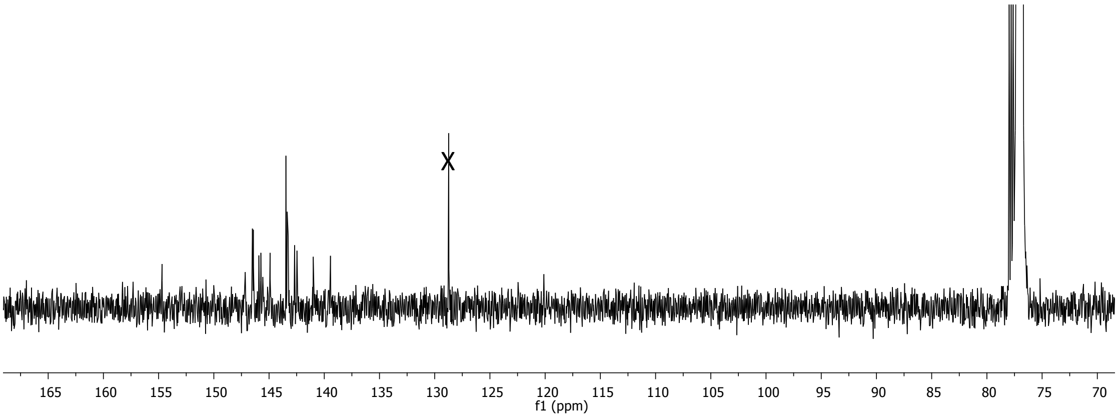

Fig. S6 ^{13}C NMR spectrum (175MHz, CS_2 with $CDCl_3$ as internal reference) **4**. Traces of benzene contained in the CS_2 were detected.

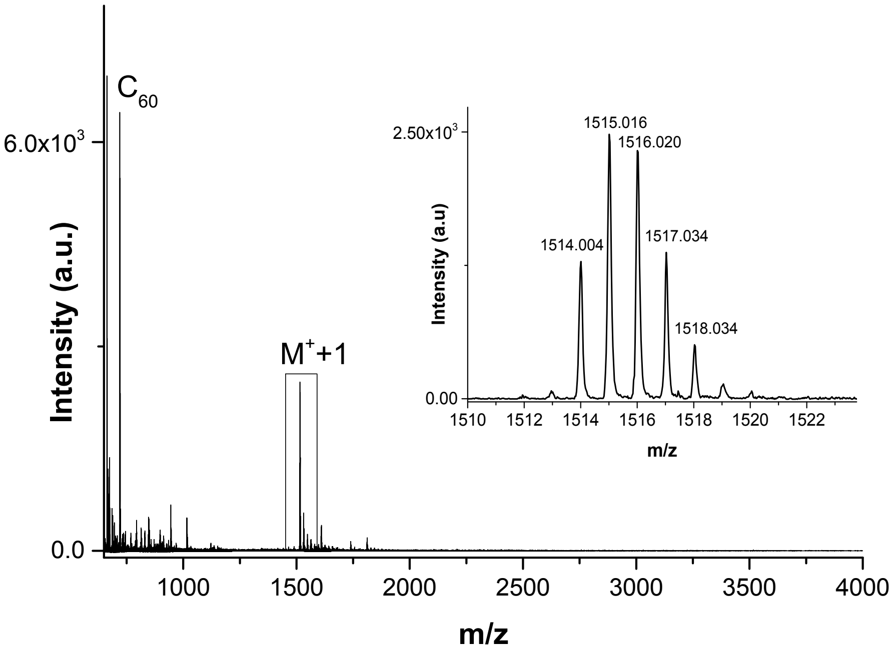

Fig. S7 EM (MALDI-TOF) of dumbbell **4**.

Generation of *fullerobenzyne* 3 and trapping with furan

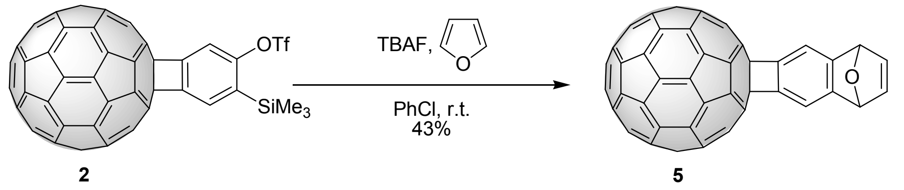

To a solution of aryne precursor **2** (120 mg, 0.12 mmol) and furan (326 mg, 4.8 mmol) in chlorobenzene (12 mL), anhydrous TBAF (1M solution in CH_3CN, 240 µL, 0.24 mmol) was dropwise added over a period of 2 h (syringe pump). The mixture was stirred at rt for 2 h. The solvent was evaporated under reduced pressure and the resulting mixture was purified by column chromatography (SiO_2, CS_2) to afford the corresponding Diels-Alder adduct **5** (44 mg, 43%) as a scarcely soluble dark solid.

^{1}H NMR (500 MHz, 313K, $CDCl_3$) δ: 7.85 (s, 2H), 7.23 (s, 2H), 5.93 (s, 2H); EM (MALDI-TOF), *m/z* (%): 862.086 (M^+, 100), 863.096 (M^++1, 90), 864.120 (M^++2, 66).

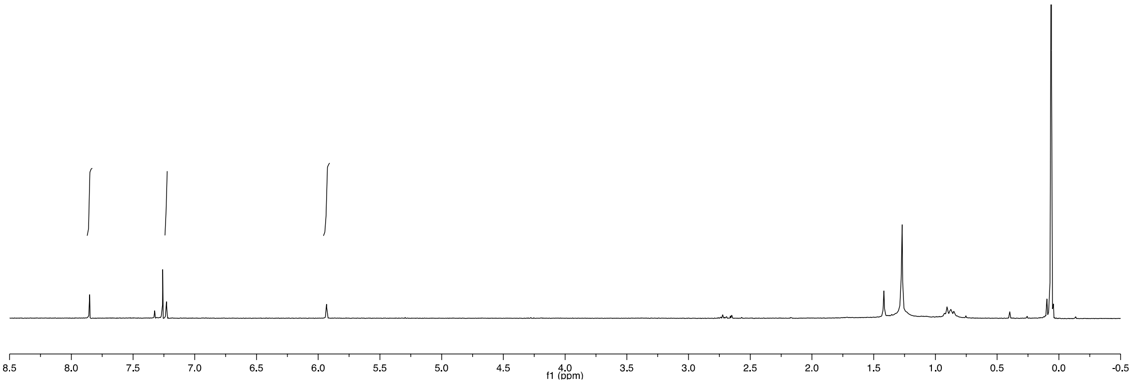

Fig. S8 ^{1}H NMR spectrum (500 MHz, $CDCl_3$) of **5**.

Generation of *fullerobenzyne* 3 and trapping with FLG: Synthesis of FLG-C_{60} nanoconjugates

Exfoliated graphene suspensions in dry *o*-DCB under argon were utilized as produced for further covalent modification (see Materials and Methods section). A solution 1 M of anhydrous TBAF in acetonitrile (2 equivalents, 0.142 mL) was slowly added dropwise (during 2 hours) to a solution of precursor **2** (50 mg, 1 equivalent) and FLG in dry *o*-DCB (100 mL). The solution was stirred vigorously for 12 hours at 40 ºC. The final product **6** was separated from the reaction mixture by filtration over a PTFE membrane (0.2 µm). The black solid was purified by subsequent washing in membrane with *o*-DCB, CH_2Cl_2, MeOH and H_2O. 6.6 mg of the of FLG-C_{60} nanoconjugates **6** were obtained. FTIR (KBr): ν = 2927, 2854, 1581, 1455, 1384, 1125, 1033, 748, 525 cm^{-1}; TGA: weight loss and temperature desorption (organic anchoring groups): 28.2%, 600 °C; Raman: I_D/I_G = 0.29; XPS: % atomic: C (284.6 eV) = 86.7, O (532.6 eV) = 13.3.

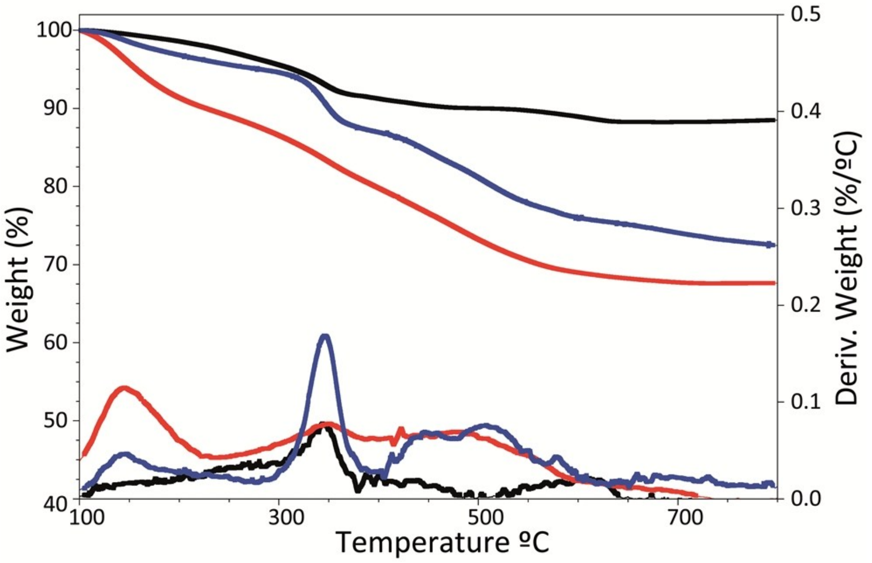

Fig. S9 TGA spectra of FLG (black), **2** (blue) and FLG-C_{60} nanoconjugates **6** (red) recorded under nitrogen atmosphere.

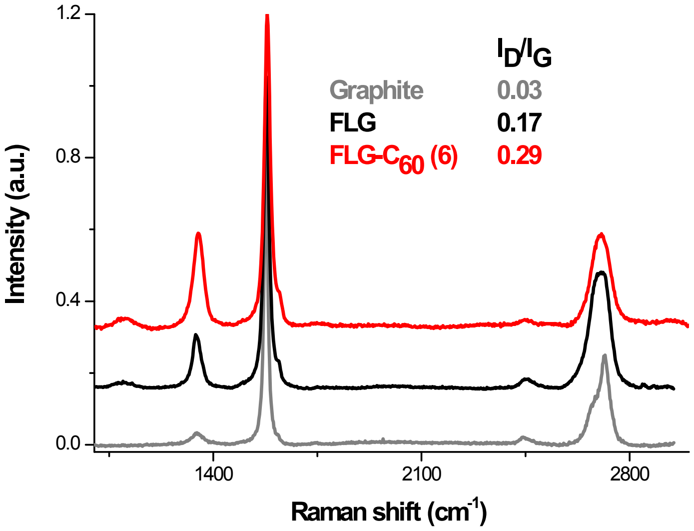

Fig. S10 Raman spectra of graphite (gray), FLG (black), and FLG-C_{60} nanoconjugates **6** (red) performed on a NT-MDT Raman apparatus under 532 nm excitation wavelength.

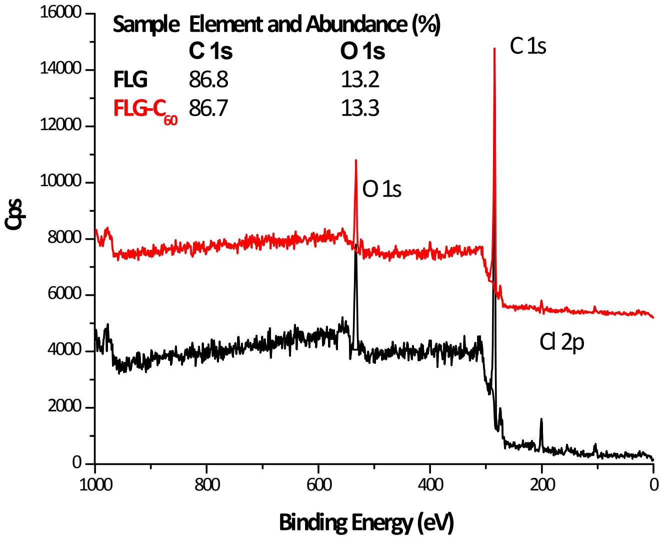

Fig. S11 XPS survey spectra for the FLG starting material (black) and the functionalized FLG-C$_{60}$ nanoconjugates **6** (red).

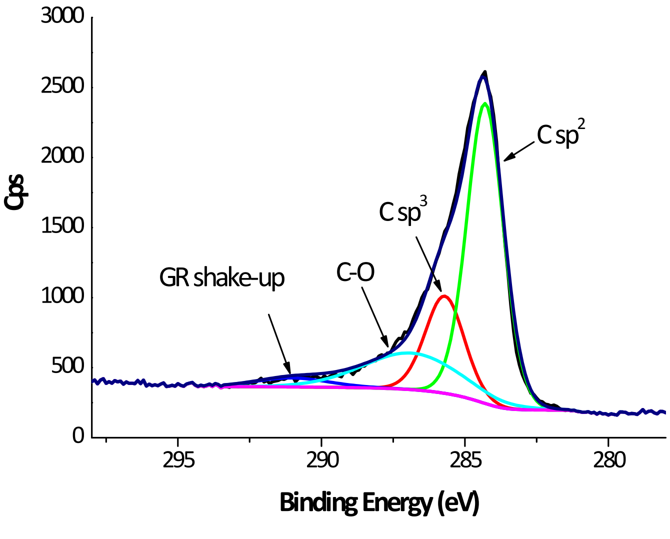

Fig. S12 C1s XPS analysis for the FLG starting material.

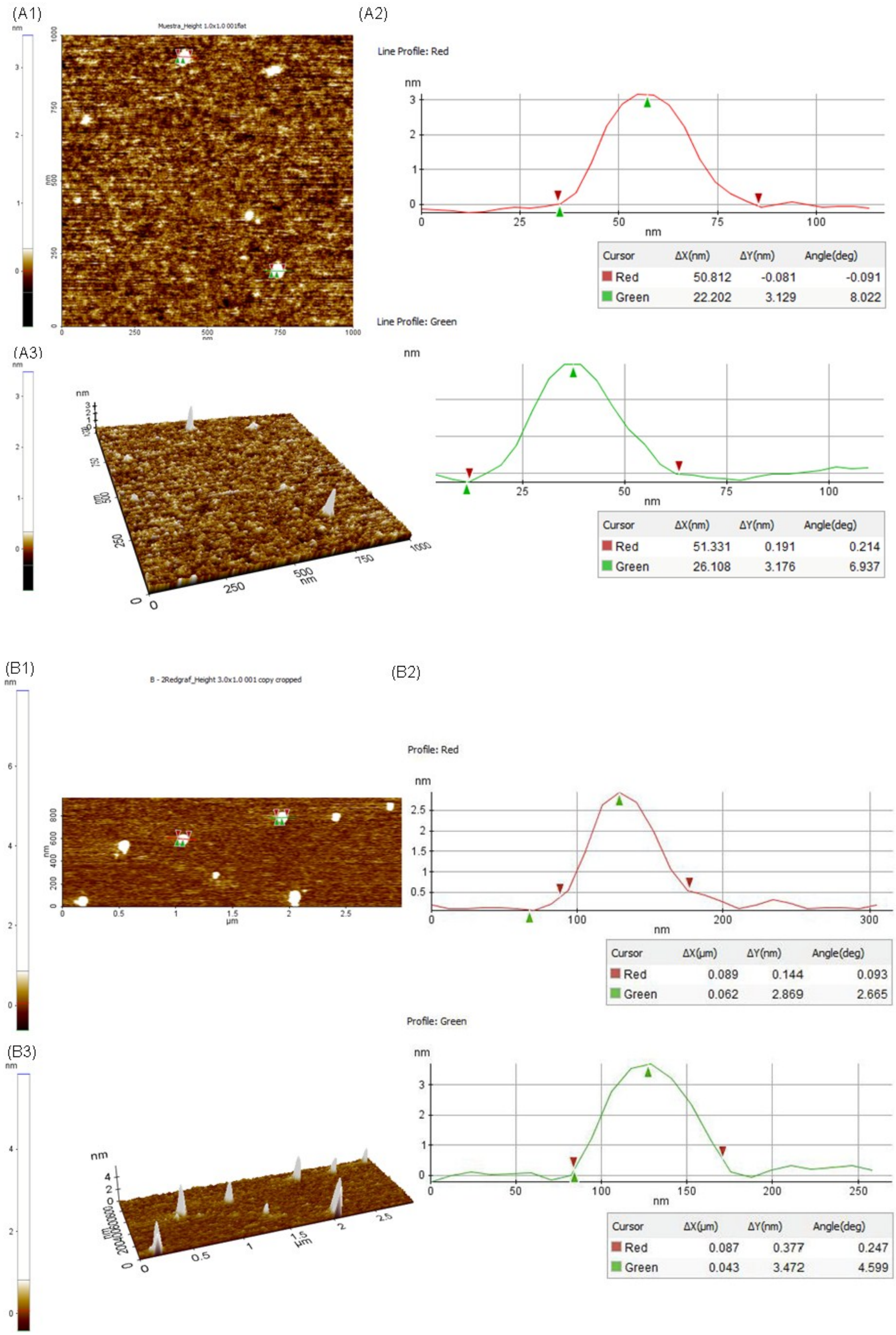

Cursor	ΔX(nm)	ΔY(nm)	Angle(deg)
🟥 Red	50.812	-0.081	-0.091
🟩 Green	22.202	3.129	8.022

Cursor	ΔX(nm)	ΔY(nm)	Angle(deg)
🟥 Red	51.331	0.191	0.214
🟩 Green	26.108	3.176	6.937

Cursor	ΔX(µm)	ΔY(nm)	Angle(deg)
🟥 Red	0.089	0.144	0.093
🟩 Green	0.062	2.869	2.665

Cursor	ΔX(µm)	ΔY(nm)	Angle(deg)
🟥 Red	0.087	0.377	0.247
🟩 Green	0.043	3.472	4.599

Fig. S13 Representative AFM images of FLG-C_{60} nanoconjugates **6**; both the 3D graphs (A3, B3) and the height profiles (A2, B2) show FLG-C_{60} flakes with 3.0-3.4 nm height.

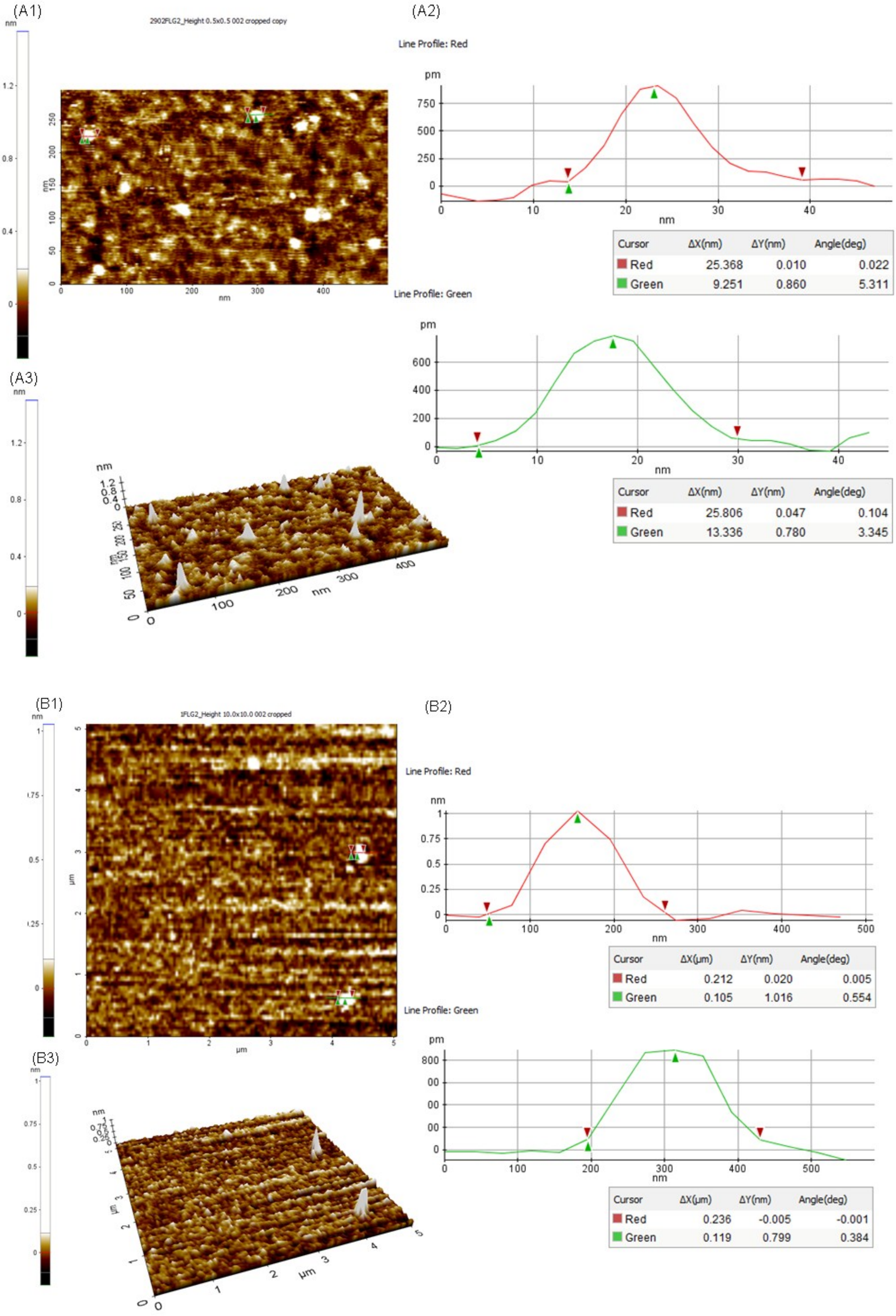

Cursor	ΔX(nm)	ΔY(nm)	Angle(deg)
🟥 Red	25.368	0.010	0.022
🟩 Green	9.251	0.860	5.311

Cursor	ΔX(nm)	ΔY(nm)	Angle(deg)
🟥 Red	25.806	0.047	0.104
🟩 Green	13.336	0.780	3.345

Cursor	ΔX(µm)	ΔY(nm)	Angle(deg)
🟥 Red	0.212	0.020	0.005
🟩 Green	0.105	1.016	0.554

Cursor	ΔX(µm)	ΔY(nm)	Angle(deg)
🟥 Red	0.236	-0.005	-0.001
🟩 Green	0.119	0.799	0.384

Fig. S14 Representative AFM images of FLG; both the 3D graphs (A3, B3) and the height profiles (A2, B2) show FLG particles with 0.8-1.0 nm height.

Computational details

The SIESTA[4] implementation of density functional theory employing a van der Waals density functional[5,6] which uses the revPBE35 revised version of Perdew, Burke and Ernzerhof generalized-gradient approximation exchange correlational functional[7] was used to investigate the energetics of the cycloaddition of benzene on a graphene surface. The van der Waals functional used in SIESTA is a universal non local density functional applicable to arbitrary geometries[8]. To ensure accuracy the inter atomic forces were relaxed to optimize the geometry to a value less than 20 meV/Å using extended double zeta polarized basis sets of pseudo atomic orbitals. In calculating the binding energies basis set superposition errors were minimized by retaining ghost states as prescribed in the counterpoise method.[9,10]

To model a few layer graphene flake (FLG) the calculations use an AB stacked bi-layer sheet of graphene of dimensions in x and y of 1.75 nm x 1.58 nm respectively giving 96 carbon atoms per sheet. Previous calculations[11] show that the bilayer increases the binding of poly aromatic hydrocarbons by ~ 6% when using the van der Waals functionals and further layers show no further increase. The bi-layer is periodic in both directions and to increase the fineness of the k point sampling a rectangular Monkhorst pack grid of dimensions 4 x 4 x 1 is employed. Furthermore to test the persistence of the connectivity trends two systems are considered namely FLG-benzyne and FLG-fullerobenzyne. The calculations are performed by removing the two hydrogens from a benzene ring to create the reactive benzyne derivative which bonds to the graphene surface when placed in proximity to the FLG surface. By starting the calculations at different reaction sites on or near to the [2+2] and [4+2] cycloadduct sites then the system can be allowed to relax to locate energy minima.

From Fig.S15 below the perpendicular separation of the FLG-benzyl moiety in the [4+2] cycloadduct configuration from the graphene surface is found to be 1.45 Å which can be compared to 1.55 Å for the FLG-benzyl moiety in the [2+2] cycloadduct configuration in Fig. S16.

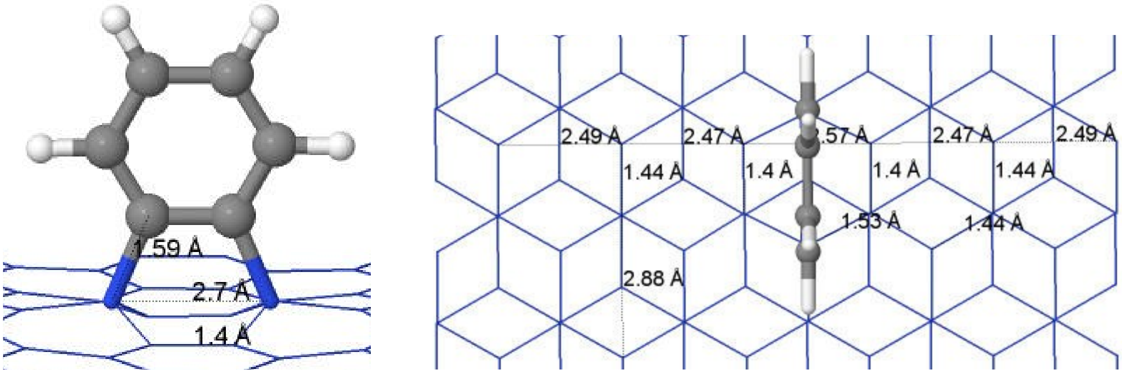

Fig. S15 The left and right hand figures present the relaxed geometry of the FLG-benzyl moiety in the [4+2] cycloadduct configuration. From the left hand figure the measurements from the associated FLG surface hexagon show the C-C bond length to be 1.40 Å and the distance across the diameter of the hexagon is 2.70 Å giving a perpendicular separation of the benzyl moiety from the associated FLG surface hexagon of 1.45 Å. The right hand figure shows the warping of the FLG surface due to the presence of the benzyl moiety.

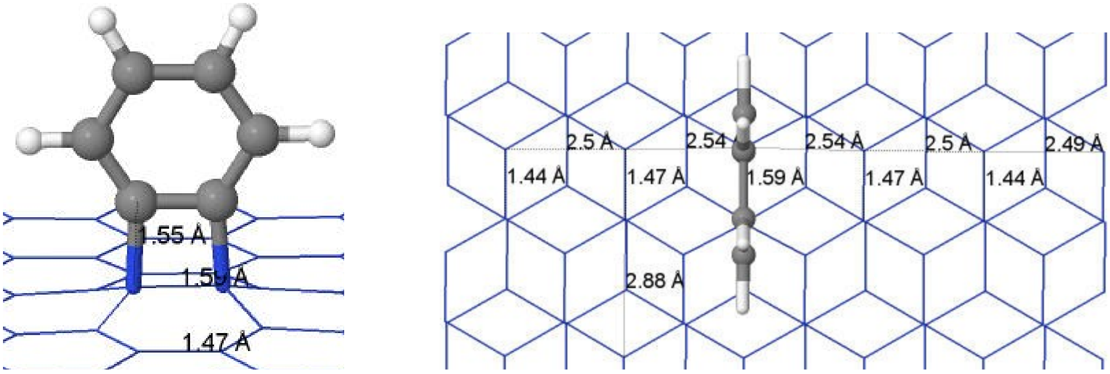

Fig. S16 The left and right hand figures present the relaxed geometry of the FLG-benzyl moiety in the [2+2] cycloadduct configuration. From the left hand figure the measurements from the associated FLG surface hexagon show the C-C bond length to be 1.59 Å with a perpendicular separation of 1.55 Å. The right hand figure shows the warping of the FLG surface due to the presence of the benzyl moiety.

As can be seen from Figs. S15 and S16 the bond lengths associated with the FLG surface hexagons in the vicinity of the benzyl moiety are subject to warping as the moiety moves from the cycloadduct positions of [4+2] to [2+2] and to further clarify the results Fig. S13 defines the location of the benzyl moiety over the FLG surface hexagon associated with the change in the binding energy. The images 1-4 show snapshots of the molecular dynamics and a movie of the molecular dynamics of the relaxation the benzyne sited at positions 5 or 13 close to the [4+2] cycloadduct is shown in image 3.

The following images are taken from snapshots of the atomic positions before (a) and (b) after relaxation to the most stable configurations of the [2+2] and [4+2] cycloaducts for FLG-benzyne. Referring to Fig. S17 defines the x axis defines the position of the benzyl moiety over an FLG surface hexagon.

1. Before relaxation the benzyne is sited at position 9 to form the [2+2] cycloadduct.

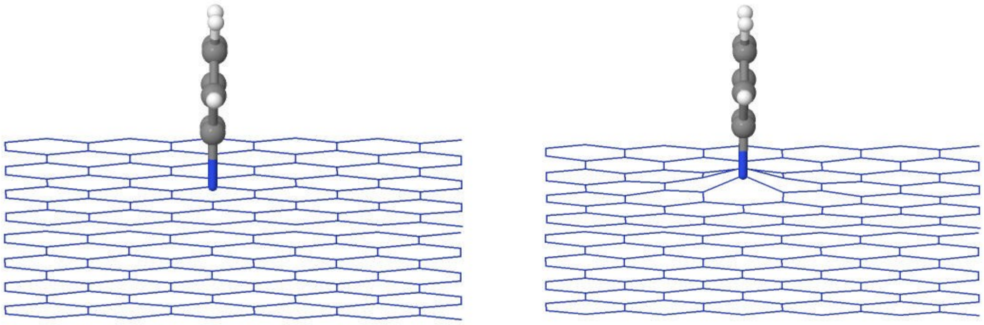

a. before relaxation

b. after relaxation

Result. The [2+2] position is stable.

2. Before relaxation the benzyne is sited at positions 2 or 16 to form the [4+2] cycloadduct.

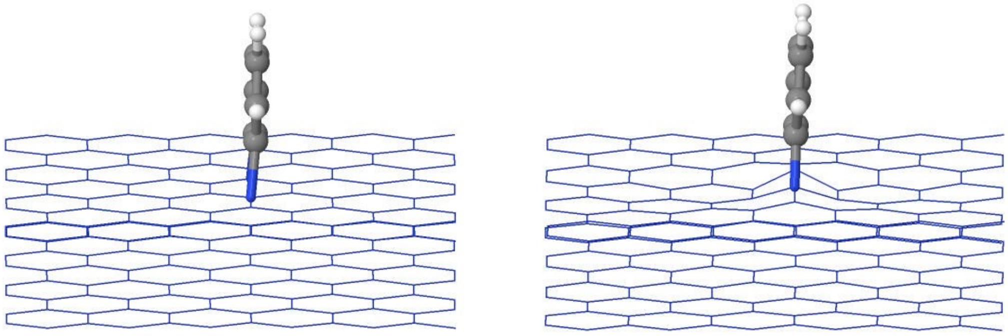

a. before relaxation

b. after relaxation

Result. The [4+2] position is stable.

3. Before relaxation the benzyne is sited at positions 5 or 13 close to the [4+2] cycloadduct.

a. before relaxation b. after relaxation

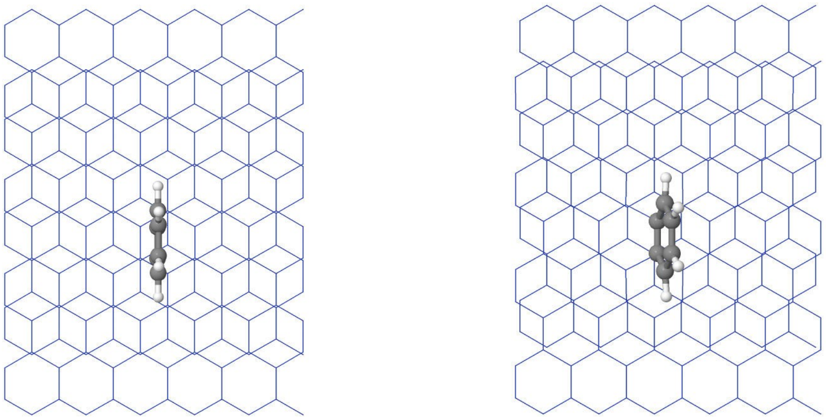

Results. The approximate [4+2] cycloaduct geometry relaxes to the [2+2] cycloadduct geometry even though the starting configuration is closer to the [4+2] than the [2+2]. Movie of this relaxation: [4+2]to[2+2].avi.

[4+2]to[2+2].avi

These trends are duplicated for the larger FLG-fullerobenzyne complex in the following snapshots.

4. Before relaxation the benzyne is sited at positions 5 or 13 close to the [4+2] cycloadduct.

a. before relaxation b. after relaxation

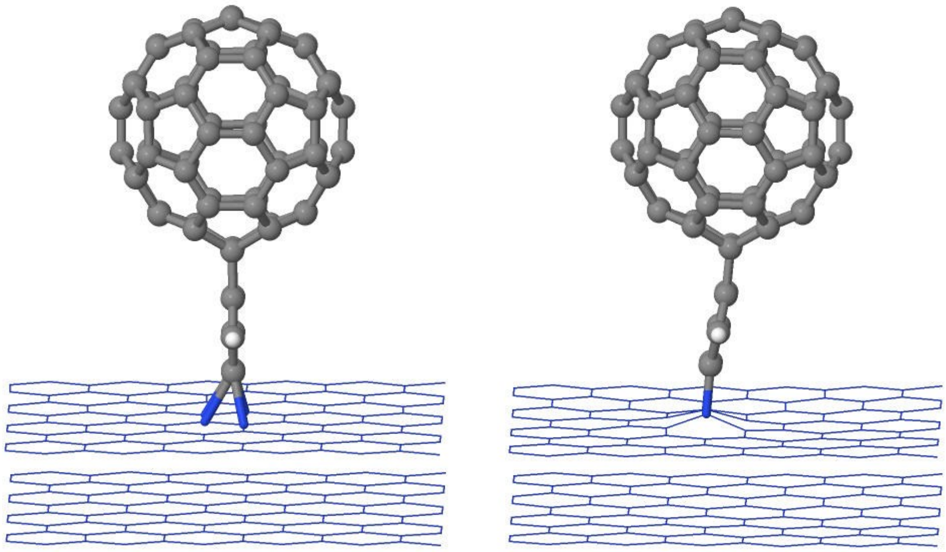

Results. The approximate [4+2] geometry relaxes to the [2+2] geometry even though the starting configuration is closer to the [4+2] than the [2+2]. The perpendicular height from the basal plane of the FLG to the C_{60} upper pentagon is 12.70 Å.

The binding energy energy (E^B eV) between the FLG and benzyne or fullerobenzyne is calculated to elliminate basis set superposition errors by using the couterpoise method of ghost states in SIESTA from:

$$E^B = E^{TOT}_{AB} - \left(E^{TOT}_{aB} + E^{TOT}_{Ab}\right) \qquad (1)$$

E^{TOT}_{AB} is the total energy of the system where A represents the FLG and B represents the benzyne or fullerobenzyne. E^{TOT}_{aB} is the total energy where the FLG is a ghost state and E^{TOT}_{Ab} the total energy where the benzyne or fullerobenzyne is a ghost state. All the reactions are found to be exothermic and the values of E^B shown in Eqn. 1 will be negative but to be consistent with the literature the bond energies are defined as the modulus: $|E^B|$ eV.

The bond energies and bond lengths for the relaxed stable configurations for the [2+2] and [4+2] cycloadduct geometries are shown in Table S1 for these exothermic reactions.

Table S1. Bond energies $|E^B|$ eV, and bond lengths *d* (Å), for the exothermic cycloadditon reaction of FLG and benzyne derivatives.

System	$|E^B|$**[2+2]**	$|E^B|$**[4+2]**	***d* [2+2]**	***d* [4+2]**
FLG-benzyne	3.63	5.67	1.55	1.59
FLG-fullerobenzyne	3.62	5.65	1.55	1.59

Table S1 shows that the most stable configuration to be the [4+2] for both systems studied.

To clarify the dynamics of the bonding Fig. S17 shows the binding energy E^B eV from Eqn. 1 plotted against position of the benzyl moiety over a graphene hexagon. All the binding energies are negative which implies an exothermic reaction. The figure shows that the [4+2] configuration is located within a steep and narrow energy minima and small deviations away from this point result in a rapid decrease in E^B, which then slowly converges towards the secondary minima located at position [2+2]. The difference in E^B between the two minima is 2.04 eV and the energy barrier to move from the minima at [2+2] to that at [4+2] is approximately 0.1 eV.

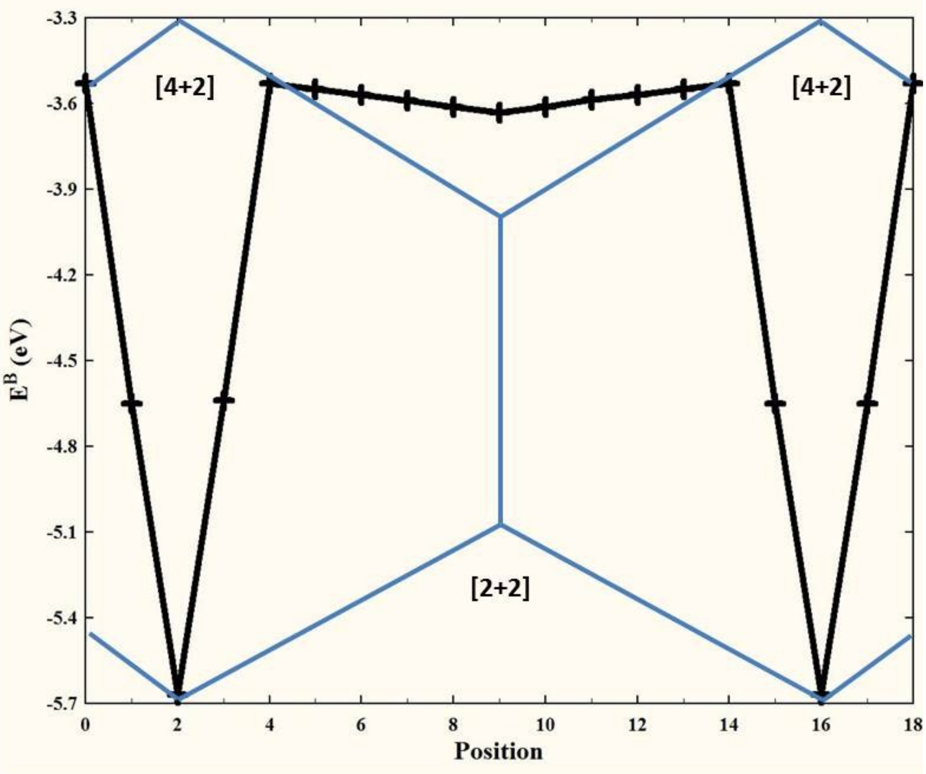

Fig. S17 The binding energy E^B is plotted as a function of location of the benzyl moiety over a graphene hexagon shown in blue. The [4+2] cycloadduct is found at positions 2 and 16 and the [2+2] cycloadduct at position 9.

As the reaction might well take place at an impurity site on the FLG upper layers the system was modelled to form a step edge as shown in Fig. S18 below. The step edge is formed by cutting the upper graphene sheet. The upper sheet is therefore no longer periodic and the edge is unsaturated which allows for distortion which simulates the step edge impurity. Table S2 compares the results with those from Table S1 for the cycloaddition on the basal plane on FLG. The values of E^B [2+2] increase as the benzyne moiety approaches the step edge whereas the values of E^B [4+2] decrease compared to the values from Table S1.

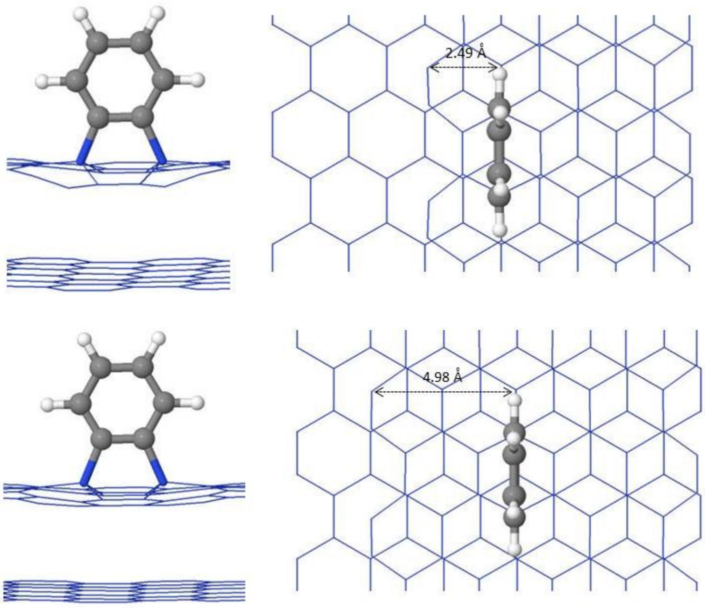

Fig. S18 The upper and lower hand figures present the relaxed geometry of the FLG-benzyl moiety in the [4+2] cycloadduct configuration. In the upper figure the cycloadduct is 2.49 Å from the step edge and in the lower figure at 4.98 Å from the step edge.

Table S2. Binding energies, E^B (eV) for the exothermic cycloadditon reaction of FLG and benzyne (FLG-benzyne). *ds* (Å) defines the distance from a graphene step edge and x defines the calculation of Table 1 where the location of the reaction occurs on an infinite plane of graphene with no step edge.

E^B [2+2]	E^B [4+2]	*ds*
4.06	5.15	2.5
4.59	5.40	5.0
3.63	5.67	x

References.

1. H. M. Duong, M. Bendikov, D. Steiger, Q. Zhang, G. Sonmez, J. Yamada and F. Wudl, *Org. Lett.,* 2003, **5**, 4433.

2. E. Yoshioka and H. Miyabe, *Tetrahedron,* 2012 **68**, 179.
3. For a similar procedure to obtain FLG in *o*-DCB, please see: C. E. Hamilton, J. R. Lomeda, Z. Z. Sun, J. M. Tour and A. R. Barron, Nano Lett., 2009, 9, 346.
4. J. M. Soler, E. Artacho, J. Gale, A. García, J. Junquera, P. Ordejón and D. Sánchez Portal, *J. Phys. Condens. Matter.,* 2002, **14**, 2745.
5. M. Dion, H. Rydberg, E. Schröder, D. C. Langreth, and B. I. Lundqvist, *Phys. Rev. Lett.,* 2004, **92**, 246401.
6. D. C. Langreth, M. Dion, H. Rydberg, E. Schröder, P. Hyldgaard, and B. I. Lundqvist, J. *Quantum Chem.,* 2005, **101**, 599.
7. M. Dion, H. Rydberg, E. Schröder, D. C. Langreth, and B. I. Lundqvist, *Phys. Rev. Lett.,* 2005, **95**, 109902(E).
8. Y. Zhang and W. Yang*, Phys. Rev. Lett.,* 1998, **80**, 890.
9. P. Jansen, H. B. Ross, and J. M. Soler*, Chem. Phys. Lett.,* 1969, **3**, 140.
10. F. Boys and S. F. Bernardi, *Mol. Phys.,* 1970, **19**, 553
11. S. Bailey, D. Visontai, C. J. Lambert, M. R. Bryce, H. Frampton and D. Chappell, *J. Chem. Phys.,* 2014, **140**, 054708.